Physics of the Earth and Planetary Interiors, 7 (1973) 349–364

PROCESSING OF MAGNETOTELLURIC DATA

JOHN F. HERMANCE
Department of Geological Sciences, Brown University, Providence, R.I. (U.S.A.)

Accepted for publication February 2, 1973

The processing of magnetotelluric data involves concepts from electromagnetic theory, time series analysis and linear systems theory for reducing natural electric and magnetic field variations recorded at the earth's surface to forms suitable for studying the electrical properties of the earth's interior.

The electromagnetic field relations lead to either a scalar transfer impedance which couples an electric component to an orthogonal magnetic component at the surface of a plane-layered earth, or a tensor transfer impedance which couples each electric component to both magnetic components in the vicinity of a lateral inhomogeneity.

A number of time series spectral analysis methods can be used for estimating the complex spectral coefficients of the various field quantities. These in turn are used for estimating the nature of the transfer function or tensor impedance. For two dimensional situations, the tensor impedance can be rotated to determine the principal directions of the electrical structure.

In general for real data, estimates of the apparent resistivity are more stable when calculated from the tensor elements rather than from simple orthogonal field ratios (Cagniard estimates), even when the fields are measured in the principal coordinates.

1. Introduction

1.1. Background

The magnetotelluric method involves determining the electrical properties of the earth's interior through the analysis of natural magnetic and telluric (electric) field variations at its surface. Basic concepts from electromagnetic theory coalesced into a practical geophysical tool through the work of Price (1950) in England, Rikitake (1946), Kato and Kikuchi (1950) in Japan, Tikhonov (1950) in Russia and Cagniard (1953) in France.

The following discussion concentrates on only one aspect of the magnetotelluric method, data processing. We do not consider the manner in which data are acquired and the problems of designing suitable magnetotelluric experiments, nor do we consider the interpretation of magnetotelluric data in terms of the electrical or geological properties of the earth.

Specifically, our intention is to review current methods by which raw data are processed to a form suitable for interpretation, without suggesting ways in which it can be interpreted.

1.2. The magnetotelluric field relations

Cagniard (1953) and Keller and Frischknecht (1966) provide excellent introductions to the theory of magnetotelluric fields over a plane-layered earth, which essentially is an out-growth of concepts from the theory of the propagation of electromagnetic plane waves in a lossy medium that is linear, homogeneous and isotropic. In such a medium an electromagnetic wave propagates so that the electric and magnetic fields vectors are orthogonal, and so that the ratio of electric to magnetic field intensity is a characteristic measure of the electromagnetic properties of the medium often called the characteristic impedance.

For a coordinate system at the earth's surface, with the axes aligned having x-north, y-east and z-down we have, for plane waves generated by sources in the ionosphere:

$$Z = \frac{E_x}{H_y} \tag{1}$$

where Z is the characteristic impedance, E_x is the electric field intensity (north) in mV/km and H_y is

the magnetic field intensity (east) in γ (10^{-5}Oe). In eq. 1 as well as in the following discussion capital letters signify frequency-domain representations, whereas lower case letters signify time-domain representations of the field quantities.

If indeed the earth is homogeneous and isotropic, then the true resistivity of the earth is related to the characteristic impedance through the relation:

$$\rho = 0.2T|Z|^2 = 0.2T\left|\frac{E_x}{H_y}\right|^2 \tag{2}$$

where ρ is the resistivity in Ω-m and T is the period in sec.

In the case of a horizontally *layered* earth (or one-dimensional earth), eq. 2 becomes an *apparent* resistivity:

$$\rho_a = 0.2T\left|\frac{E_x}{H_y}\right|^2 \tag{3}$$

which is frequency-dependent. For example, if the earth consisted of two layers, the finite depth of penetration of the fields would cause eq. 3 to be asymptotic to the resistivity of layer 1 at short periods and asymptotic to the resistivity of layer 2 at long periods.

Moreover, because of the symmetry of the problem, estimates of the characteristic impedance for either a homogeneous or a *layered* earth do not depend on rotation of the measuring axes in the horizontal plane, so that the north and east electric components are related to the orthogonal magnetic components through the linear equations:

$$E_x = Z H_y \text{ and } E_y = -Z H_x \tag{4}$$

Each of these equations is a statement of the condition that at a particular period an *electric* field component is linearly related to its orthogonal *magnetic* field component through a single-valued complex scalar transfer function. This is a direct analog from simple filter theory. The output signal of a filter (E_x) is linearly related to the input signal (H_y) multiplied by the frequency response of the filter (Z).

The relation (eq. 3) was formulated for the first time by Cagniard (1953) and as a result is known as the Cagniard *relation*. The conditions under which eq. 3 is valid are called the Cagniard *conditions*. They are that the incident electromagnetic fields are plane waves at the earth's surface and that the earth consists of parallel plane layers.

In regions where the earth has a more complicated structure than simple plane layers, the coupling between electric and magnetic fields is more complicated. As an example, electric fields may be strongly distorted near a lateral inhomogeneity whereas magnetic fields may be relatively undistorted. The electric field is then locally polarized at some angle other than 90° to the regional magnetic field. At each point in the vicinity of the lateral discontinuity, this results in a linear coupling of *each* electric field component to a combination of *both* magnetic field components of the form:

$$E_x = a H_x + b H_y \tag{5}$$

where a and b are called coupling coefficients which, as might be expected, depend on position, coordinate direction, period and the geometry and electrical properties of the lateral inhomogeneity.

Defining an impedance tensor in the following way:

$$[Z] = \begin{bmatrix} Z_{xx} & Z_{xy} \\ Z_{yx} & Z_{yy} \end{bmatrix} \tag{6}$$

we can generalize eq. 5 to a relation of the form $E = [Z] \cdot H$ or:

$$E_x = Z_{xx}H_x + Z_{xy}H_y \text{ and } E_y = Z_{yx}H_x + Z_{yy}H_y \tag{7}$$

However, for a strictly two-dimensional geometry, Maxwell's equations separate into two modes (Cantwell, 1960; Kovtun, 1961; Bostick and Smith, 1962). In one mode, E-parallel to strike depends only on H-perpendicular to strike, and in the other mode, E-perpendicular to strike depends only on H-parallel to strike.

In this case, the tensor decouples into two modes represented by:

$$E'_x = Z'_{xy}H'_y \text{ and } E'_y = Z'_{yx}H'_x \tag{8}$$

where the prime indicates that the measuring axes (X, Y) are aligned parallel and perpendicular to the strike of the two-dimensional, lateral inhomogeneity. This special orientation (x', y') is called the principal coordinate system and Z'_{xy} and Z'_{yx} are called the principal impedance values.

For arbitrary orientations of the measuring axes away from the principal directions one finds, as might be expected a linear coupling of *each* electric

component to both magnetic components expressed by the tensor formulation in eq. 7.

Rotating the new measuring coordinates away from the principal directions through an angle measured in the clockwise sense looking down, the new tensor elements expressed in terms of the principal values (Z'_{xy}, Z'_{yx}) and the rotation angle θ are:

$$\left.\begin{aligned} Z_{xx} &= (Z'_{xy} + Z'_{yx}) \sin 2\theta/2 \\ Z_{xy} &= Z'_{xy} - (Z'_{xy} + Z'_{yx}) \sin^2\theta \\ Z_{yx} &= Z'_{yx} - (Z'_{xy} + Z'_{yx}) \sin^2\theta \\ Z_{yy} &= -(Z'_{xy} + Z'_{yx}) \sin 2\theta/2 \end{aligned}\right| \quad (9)$$

From inspection of these tensor elements several properties appear obvious:

$$Z_{xx} = -Z_{yy} \quad (10)$$

and:

$$Z_{xy} - Z_{yx} = \text{constant} \quad (11)$$

at *all* rotation angles. During rotation through 180°, the off-diagonal elements (Z_{xy}, Z_{yx}) each go through one maximum and one minimum. The diagonal elements (Z_{xx}, Z_{yy}) each go through two minima. For a purely two-dimensional situation the diagonal elements go through zero every time the rotating coordinate system passes through a principal direction.

The values of the off-diagonal tensor elements (Z'_{xy}, Z'_{yx}) in the principal coordinates are used for estimating the principal resistivity values (ρ'_{xy}, ρ'_{yx}), one of which is maximum and the other minimum.

2. Data processing

2.1. Spectral analysis of time series

Since the interpretation of magnetotelluric data is usually done in the frequency domain, spectral analysis of the raw data is an important aspect of data processing. This involves creating a time series x_j, by sampling a signal $x(t)$, at equal intervals of time Δt, from $j = 1$ to N, where $T_0 = (N - 1)\,\Delta t$ is the duration of the signal.

One intuitively feels that for the sampled data to represent the original signal adequately, the signal should be smooth over the sampling interval, Δt. In a more rigorous sense, an absolute requirement is that the signal to be sampled should have negligible spectral energy at periods shorter than twice the sampling interval (or at frequencies above the Nyquist frequency $(1/2\Delta t)$).

There are a number of techniques for transforming the time series into spectral information in the frequency domain. Although in principle, all of these methods are equivalent, since they result in the Fourier components of the record, in practice there are important differences that depend on the character of the signal and the underlying assumptions regarding the nature of the data. Clearly, physical insight should override a strict mathematical application of any of these methods.

2.1.1. Fourier harmonic analysis

The fundamental assumption in Fourier harmonic analysis is that the time series of length T_0 is cyclic or periodic with fundamental period T_0, such that $x(t) = x(t + T_0)$. This assumption places strict constraints on the spacing between harmonics as well as implying that the record section can be optimally approximated over its length T_0 by a *finite* number of harmonics. This can be seen in the following way. Over an interval of time $(-T_0/2, T_0/2)$ a function $x(t)$ can be expressed as the sum of a Fourier series:

$$x(t) = \sum_{k=-\infty}^{k=+\infty} X_k \, e^{ik\omega_0 t}, \quad \omega_0 = \frac{2\pi}{T_0} \quad (12a)$$

where X_k is given by:

$$X_k = \frac{1}{T_0} \int_{-\frac{T_0}{2}}^{\frac{T_0}{2}} x(t)\, e^{-ik\omega_0 t}\, dt \quad (12b)$$

The amplitude spectral lines X_k are spaced at intervals k/T_0 along the frequency axis, which are harmonics of the record length T_0. Since we have required that the signal $x(t)$ be band-limited to frequencies less than the folding-frequency $(1/2\Delta t)$, and since $T_0 = (N - 1)\,\Delta t$, the maximum harmonic is $k_{max} = (N-1)/2$. However, in eq. 12a, since we allow both positive and negative harmonics, as well as a term for $k = 0$, the total number of harmonics needed is N, the same as our number of data points.

The Fast-Fourier Transform (F.F.T.) is simply a high speed algorithm for calculating the N complex Fourier harmonic coefficients (Cooley and Tukey, 1965; Bergland, 1969), and for large time series it pro-

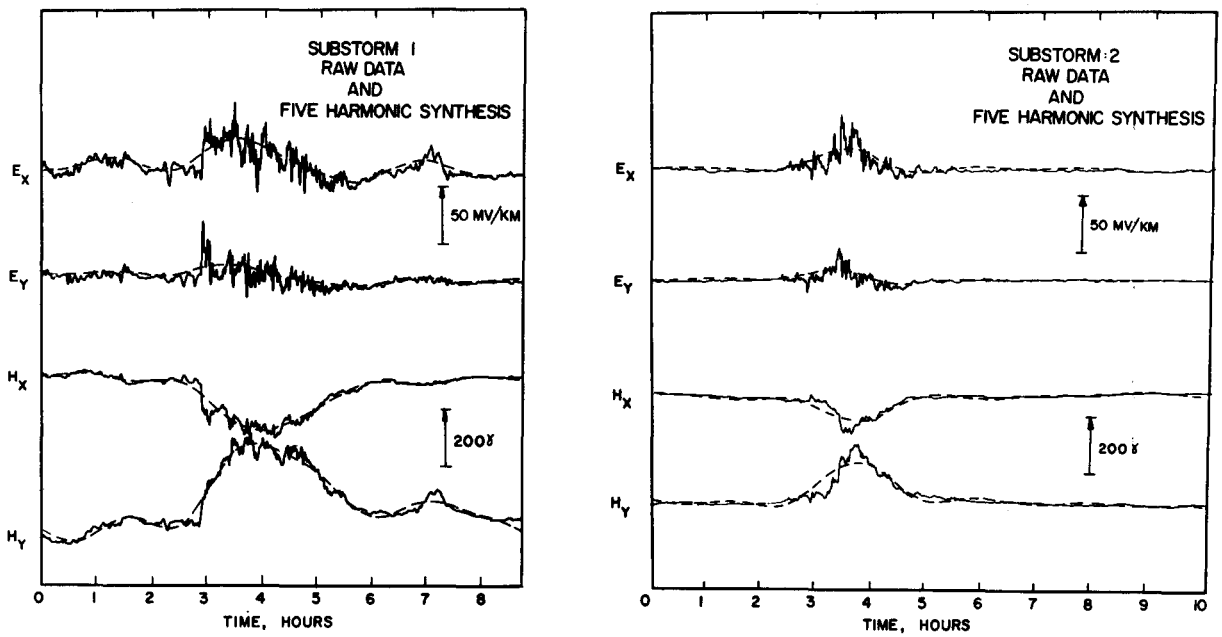

Fig. 1. Magnetotelluric field components from two magnetic substorms. The dashed lines represent new time series synthesized from first five harmonics of original time series. Data from southwest Iceland (Thingvellir).

vides a major saving in computer cost and time compared with using conventional techniques. However, no few information is obtained from the F.F.T.—just cheaper information. On the other hand, if one does not want the entire spectrum but only a few closely spaced spectral estimates in a particular frequency band, the F.F.T. may actually be more expensive to run.

Whichever scheme one chooses to use for calculating the harmonic coefficients, the point is that the synthesis of a new time series from these N harmonics precisely equals $x(t)$ at the intervals $t = (j-1)\,\Delta t$; $j = 1, N$.

On the other hand, the synthesis of only a few harmonics rather than all N harmonics still approximates the original time series in the least-squares sense but does not look like $x(t)$ in detail. In fact, we can use the first few harmonics to obtain a smooth version of the actual time series as shown in Fig. 1 where we have synthesized a new set of time series using the first five harmonics for each of the original components shown. In this way we can study the behavior of long-period phenomena, which might otherwise be buried in noise.

In Fig. 2 we show the projection of the disturbance vectors of substorm 2 in Fig. 1 on to the horizontal plane. Electric field polarizations are shown in the top circle of each set and magnetic field polarizations are shown in the bottom circle. The raw data are shown, as well as the new time series discussed above, which was synthesized from the first five harmonics of the original series. We also show the band-pass filtered data to be discussed in a later section. The vertical axis in all plots represents a direction 57° east of the geomagnetic meridian.

Although the raw data show a confused polarization caused by dominant short-period signals, particularly on the electric channels, the long-period data clearly show orthogonally polarized events for the electric and magnetic fields, respectively.

We have obtained Cagniard estimates at these long periods by substituting into eq. 3 the electric and magnetic field amplitudes for components measured along the major axis of the respective polarization ellipse. Apparent resistivities obtained in this way for the two events shown in Fig. 1 are given in Table I. The agreement between the two substorms appears to be substantially improved when the raw data are linearly detrended before calculating the Fourier coefficients. However, the first harmonic, in particular, seems to

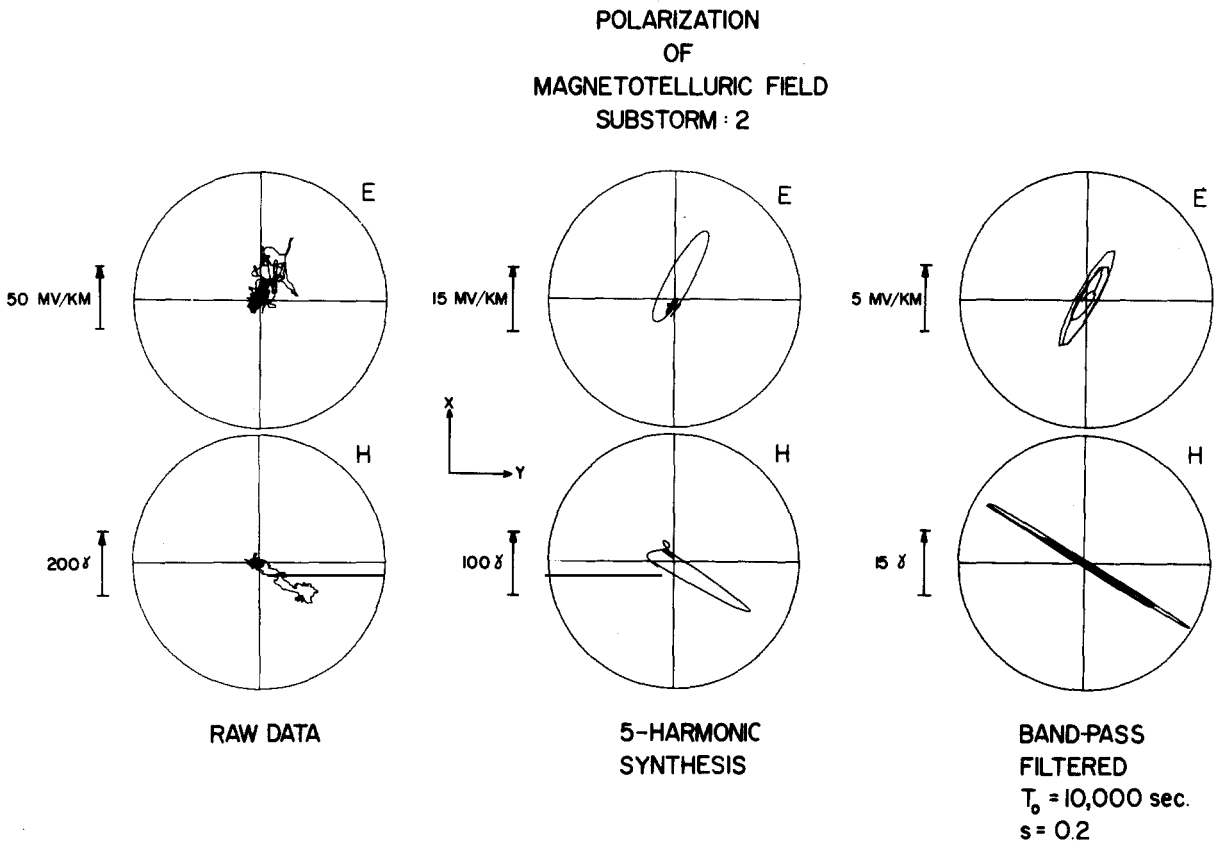

Fig. 2. Polarization plots obtained by projecting the tips of disturbance vectors of substorm 2 onto horizontal plane. Electric field polarizations are shown in the top circles, magnetic field polarizations are shown in the bottom circles. Left to right are the raw data, the new time series synthesized from first 5 Fourier harmonic coefficients, the time series band-pass filtered at 10,000 sec with a selectivity of 0.2

TABLE I

Cagniard apparent resistivities from Fourier coefficients of components along major axes of polarization ellipses

Harmonic Number	Substorm 1		Substorm 2	
	Period (sec)	ρ_a (Ω-m)	Period (sec)	ρ_a (Ω-m)
1	33600	18* (24)	36500	38* (60)
2	16800	45 (30)	18300	52 (37)
3	11200	57 (68)	12200	49 (55)
4	8400	40 (15)	9100	43 (46)
5	6700	43 (35)	7300	42 (34)

Site: Thingvellir (S.W. Iceland). Raw data were linearly detrended. Brackets denote estimates for data not detrended.

* First harmonic will be extremely sensitive to detrending function and is not used in final interpretation

be extremely sensitive to the detrending function chosen, and does not lead to consistent apparent resistivities between two sets of data.

2.1.2. Fourier transient analysis

Although the harmonic analysis discussed above precisely represents the original time series over the record length T_0, providing N coefficients are used, a question which is sometimes important is what happens outside of the range T_0. Is the signal indeed cyclic with fundamental period T_0, as assumed in harmonic analysis, is it stationary in the statistical sense, or is it a transient?

In the case of a magnetic substorm, for example, we know we are dealing with a transient phenomenon. It is not periodic, and unless our record includes many

days of continuous record, it is not stationary. To represent adequately our time series over all time (not only over the record length T_0) we not only need spectral estimates at discrete multiples of the fundamental frequency, but at all frequencies in between, so that we have a continuous spectrum which can be calculated from the Fourier transform pair:

$$x(t) = \frac{1}{2\pi} \int_{-\infty}^{\infty} X(\omega)\, e^{i\omega t}\, d\omega$$

$$X(\omega) = \int_{-\infty}^{\infty} x(t)\, e^{-i\omega t}\, dt \qquad (13)$$

The reason that we were permitted to calculate Fourier *harmonic* coefficients for essentially *transient* phenomena, as we did in section 2.1.1 for the two magnetic substorms, is that the harmonic coefficients precisely equal the transient coefficients calculated from eq. 13 except for a scaling factor that cancels when field ratios are taken, as in calculating impedance values. However, unlike the spectrum of a periodic signal, which consists of a series of spectral peaks along the frequency axis at intervals of $1/T_0$, the spectrum of a transient function is a continuum of energy.

Fourier transient analysis has useful features in some cases. For example, at very long periods one might want to average spectral components over a finite band-width but find harmonics from the F.F.T. too widely spaced to have similar characteristics for averaging. If upon close inspection the signal is a transient phenomenon and essentially zero outside the range $t = 0$ to $t = T_0$, the Fourier coefficients at arbitrary and convenient intervals can be averaged over the band-width desired, providing only that the spectrum is smooth enough for the average to be meaningful.

2.1.3. Power spectral analysis

The term power spectral analysis usually refers to an algorithm that uses the Fourier transform of the autocorrelation or cross-correlation function in the time domain (Blackman and Tukey, 1959; Jenkins and Watts, 1968). Interest in this method grew out of statistical communication theory developed in the late 1940's and early 50's. Applications of statistical communication theory to geophysics were strongly influenced by the activity of the M.I.T. Geophysical Analysis Group in the mid-1950's. By the early 1960's these methods were being routinely applied to the processing of magnetotelluric data (Cantwell, 1960; Bostick and Smith, 1962; Vozoff et al., 1963; Srivastava et al., 1963; Madden, 1964).

The application of power spectral techniques to magnetotelluric data has generally been done under the assumption that the time series were stationary random processes, although this characteristic was seldom tested. Jenkins (1961) observes that there appear to be three types of time series which arise in practice: (1) "those which exhibit stationary properties over fairly *long* periods . . . "; (2) "those which are reasonably stationary if examined over a sufficiently *short* period . . . "; and (3) "those for which the stationary assumptions are manifestly *untrue*." The latter category emphasizes the caution an investigator must display in applying criteria from theoretical statistics to real time-series data.

However, the fact that certain time series are more like transient phenomena than stationary phenomena does not preclude their power-spectral analysis (or more precisely, energy-spectral analysis). Correlation functions and their Fourier transforms are well-defined for transient phenomena (Lee, 1963), so that it is difficult to understand an apparent preoccupation in the literature with applying the stationary-time series analysis approach of Blackman and Tukey (1959) to what very often are transient signals. Alternative approaches are possible, if not required.

The cross-correlation function of two transient signals, $x(t)$ and $y(t)$, is defined as:

$$p_{xy}(\tau) = \int_{-\infty}^{\infty} x(t)\, y(t+\tau)\, dt \qquad (14a)$$

which has the Fourier transform (called the cross-energy density spectrum):

$$P_{xy}(\omega) = \int_{-\infty}^{\infty} p_{xy}(\tau)\, e^{-i\omega\tau}\, d\tau \qquad (14b)$$

By writing $y(t+\tau)$ in eq. 14a as a Fourier transform:

$$y(t+\tau) = \frac{1}{2\pi} \int_{-\infty}^{\infty} Y(\omega) e^{i\omega(t+\tau)}\, d\omega$$

and changing the order of integration, eq. 14a becomes:

$$p_{xy}(\tau) = \frac{1}{2\pi} \int_{-\infty}^{\infty} Y(\omega) \left[\int_{-\infty}^{\infty} x(t)\, e^{i\omega t}\, dt \right] e^{i\omega\tau}\, d\omega$$

or:

$$p_{xy}(\tau) = \frac{1}{2\pi} \int_{-\infty}^{\infty} X^*(\omega)\, Y(\omega)\, e^{i\omega\tau}\, d\omega \qquad (15)$$

where the star (*) denotes the complex conjugate. Taking the Fourier transform of eq. 15 and comparing it with eq. 14b, we see that:

$$P_{xy}(\omega) = X^*(\omega)\, Y(\omega) \qquad (16)$$

which relates the cross-energy density spectrum of two transient signals to the product of the Fourier transform coefficients of the individual signals.

If, on the other hand, we are indeed dealing with stationary random processes then the cross-correlation function is defined as:

$$p_{xy}(\tau) = \lim_{T\to\infty} \frac{1}{T} \int_{-T/2}^{T/2} x(t) y(t+\tau)\, dt \qquad (17a)$$

where the Fourier transform of eq. 17a is just the cross-power spectrum:

$$P_{xy}(\omega) = \int_{-\infty}^{\infty} p_{xy}(\tau)\, e^{-i\omega\tau}\, d\tau \qquad (17b)$$

The discrete sample representations of equation set (14) and of equation set (17) are significantly different for most applications and one should tailor the analysis technique to the physical process occurring. For example, equation set (17) may be useful for investigation broad-band day-time micropulsation data whereas equation set (14) is a more meaningful way to investigate transient substorm phenomena.

2.1.4. Band-pass filtering

Each of the three techniques above, *harmonic* analysis, *transient* analysis and *power spectral* analysis, provides spectral information on the entire record section that is to say each Fourier coefficient is a least-squares approximation to the entire length of the data T_0. In a sense there are *average* spectral components.

It is not all clear that this is always the most effective way to investigate a time series, in particular, if upon inspection of the record it appears that certain frequency components are impulsive in origin and not continuous down the record. By calculating a spectral component for the entire record we average short signal bursts with long periods of quiescence. Even though there is no signal during the quiescent periods, we still effectively integrate any noise contribution into our Fourier coefficient, thus degrading the significance of the spectral estimate.

The motivation for using digital band-pass filter techniques is to incorporate into the analysis spectral estimates as a function of time, selecting sections of record that have high signal levels and rejecting sections that have low signal levels. Present applications of this technique developed from contemporaneous, though apparently independent, work of Swift (1967), Morrison et al. (1968), and Hermance and Garland (1968).

There are three popular algorithms for calculating digital band-pass filtered data. They are:

(1) Convolution between the input time series and a filter impulse response.

(2) Recursive techniques using properties of the z-transform.

(3) Using the Fast Fourier Transform to transform the time series into the frequency domain, then multiplying by a complex filter response and transforming the product back to the time domain.

The last of these techniques, although practical because of the high speed of the F.F.T.-algorithm, has not found wide use in the magnetotelluric literature and will not be discussed in detail. We shall concentrate on the first two techniques.

Convolution filtering is an algorithm based on the convolution integral:

$$y(t) = \int_{-\infty}^{\infty} h(t-\tau)\, x(\tau)\, d\tau \qquad (18)$$

where $x(t)$ is the original time series, $h(t)$ is the impulse response function of the filter function and $y(t)$ is the output of the filtering operation. To illustrate an application of this method, the frequency response of a typical filter is shown in Fig. 3. The response function is:

$$H(\omega) = e^{-(\omega-\omega_0)^2/s^2} + e^{-(\omega+\omega_0)^2/s^2} \qquad (19)$$

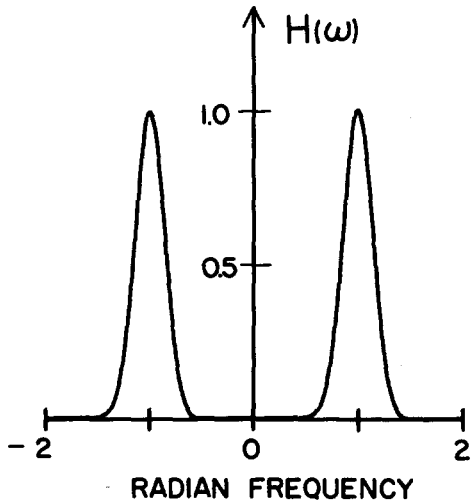

Fig. 3. The frequency response function used in our particular convolution-filter. The center frequency is 1 radian/sec and the selectivity is 0.2.

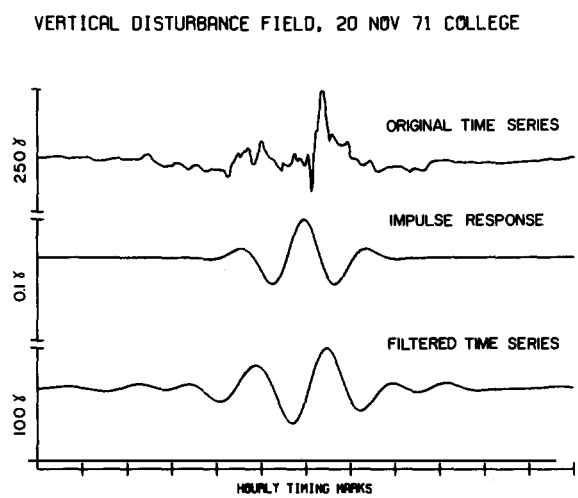

Fig. 4. Example of convolution-filter applied to magnetic substorm data. From top to bottom, we show the raw disturbed Z-field, the impulse response function, and the filtered Z-field.

where the center frequency (ω_0) is 1 radian/sec and the selectivity (s) is 0.2 ω_0. The response of the filter is unity at the center period.

The Fourier transform of eq. 19 is the impulse response shown in Fig. 4, which is an example of the technique applied to magnetic substorm data from the standard observatory at College, Alaska. We show the disturbed z-field, the impulse response function, which is convolved with the original time series, and the resultant time series, which is the output of our band-pass filter.

The correlation between the raw input series and the output filtered series is quite obvious. The output is not only smoothed, but it is band-limited. We have eliminated the high-frequency fluctuations as well as long-period trends. As another example, we have band-passed both substorm 1 and substorm 2 (Fig. 1) at a period of 10^4 sec and a selectivity of 0.2. The projection of the band-passed magnetotelluric disturbance vectors for substorm 2 on to the horizontal plane is shown in Fig. 2 along with data discussed in section 2.1.1. There is a strong orthogonal polarization of the electric and magnetic field ellipses.

Amplitudes of the filtered data projected on to the major axis of the respective polarization ellipse in Fig. 2 were substituted into eq. 3 to estimate the Cagniard apparent resistivities. The results are summarized in Table II for both substorms using three peak amplitude values for each substorm. The apparent resistivities in Table II agree remarkably well with the estimates from the Fourier transform given in Table I.

The second type of filter we intend to discuss is the digital recursive filter. This class of filtering techniques is simply the application of a high-speed algorithm which relies on special properties of the z-transform of sampled time series. An underlying assumption is that the time series is discrete and periodic in time (with period T_0) and the frequency spectrum is discrete and periodic in frequency (with period of twice the folding frequency). The theory of the z-transform is given by Jury (1964), where an introduction to digital recursive filtering is given by Shanks (1967).

TABLE II
Cagniard apparent resistivities from amplitudes of band-pass filtered data along the major axes of polarization ellipses

Amplitude number	Substorm 1	Substorm 2
	ρ_a (Ω-m)	ρ_a (Ω-m)
1	34	43
2	41	45
3	48	46

Site: Thingvellir (S.W. Iceland). Center period = 10,000 sec. Selectivity = 0.2.

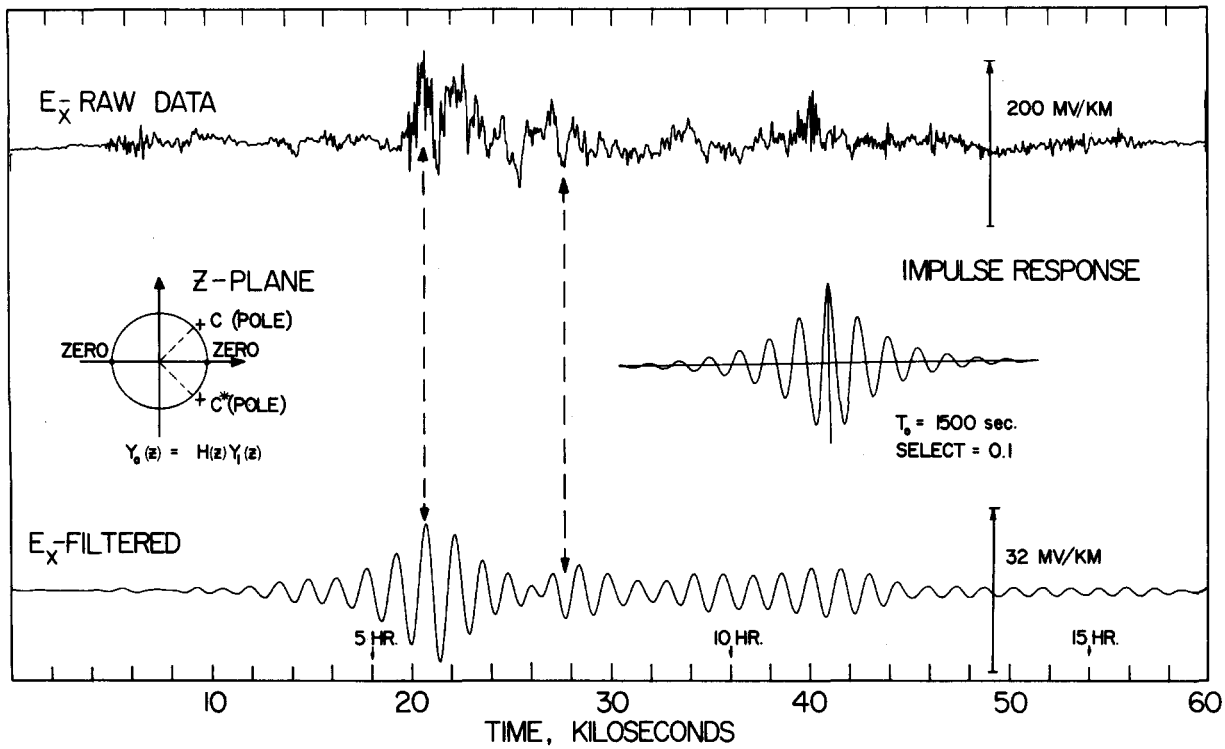

Fig. 5. Application of digital recursive filters to electric field data from Iceland. At center-left we show the z-plane representation of the particular response. At center-right we show the impulse response representation of the same filter. Raw data are shown in the top trace, filtered data in the bottom trace.

In Fig. 5 we illustrate the z-plane characteristics of a filter function that we have found particularly useful, as well as the result of operating on raw electric field data. The z-transform of the filter function consists of two poles symmetric about the origin and two zeros as shown. The displacement of each pole off the unit circle is a measure of the selectivity of the filter response. The recursive operation of the filter function on the raw data generates the filtered output series.

The primary advantage of digital recursive filters is the greater speed of the algorithm since the output of a recursive filter is exactly what one would get from a convolution type filter. This is stressed in Fig. 5 by sketching the impulse response of the same filter used in the recursive operation. The dashed arrows between the raw and filtered data attempt to draw attention to phases in the raw data that correlate with phases in the filtered data. The use of digital recursive filters in preference to convolution type filters at long periods, has decreased the cost of a computer run from $25. U.S. to $2. U.S.

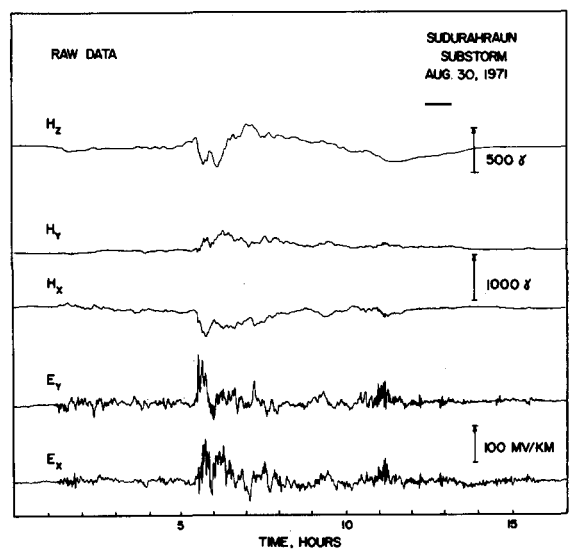

Fig. 6. Magnetotelluric components along geographic coordinates from magnetic substorm recorded in north-central Iceland (Sudurárhraun). Long-period phases in the beginning of record correlate well between components.

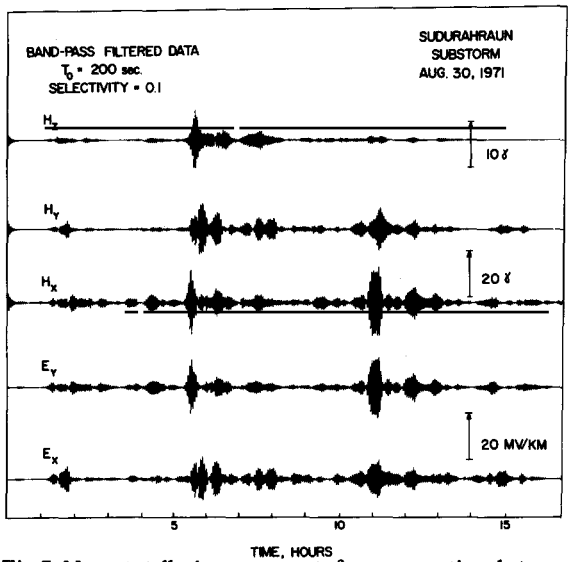

Fig. 7. Magnetotelluric components from magnetic substorm of Fig. 6 band-pass filtered at 200-sec period with selectivity 0.1. Correlation of events between orthogonal magnetotelluric pairs (E_x, H_y or E_y, H_x) is remarkably clear.

An important application of digital filters is to clean up data for visual inspection of quality and correlation. In Fig. 6 we show a five-component set of magnetotelluric records about 15 hours long from North-Central Iceland. The recordings are shown in geographic coordinates. From bottom to top we have Electric-north, Electric-east, Magnetic-north, Magnetic-east and Magnetic-vertical down.

It is fairly clear that long-period events correlate on this record. Whereas bursts of signal seen on the electric components having periods of the order of 200 sec near the beginning of the substorm and in its later phases are not clearly correlated with magnetic activity. By band-pass filtering the data at the period of interest, or 200 sec, these correlations are very clear as shown in Fig. 7.

Not only do the bursts correlate between orthogonal electric and magnetic fields as they should, but the *envelopes* on orthogonal components are remarkably similar, while the envelopes on parallel electric and magnetic components are grossly dissimilar.

2.2. Estimating the tensor elements

Having described in the last section various methods for converting time series into spectral amplitude information, we now turn to methods for estimating the tensor elements of eq. 6 from spectral amplitudes of the magnetotelluric field components.

2.2.1. Estimates from two independent record sets

Cantwell (1960) proposed a method for estimating the tensor elements by taking the Fourier transform of two independent sets of records of e_x, e_y, h_x and h_y. Denoting these data sets by I and II respectively, the electric field component in the x-direction, as an example, can be written in terms of its spectral estimate from both data sets as:

$$\left.\begin{aligned} E_x^{\mathrm{I}} &= Z_{xx} H_x^{\mathrm{I}} + Z_{xy} H_y^{\mathrm{I}} \\ E_x^{\mathrm{II}} &= Z_{xx} H_x^{\mathrm{II}} + Z_{xy} H_y^{\mathrm{II}} \end{aligned}\right| \qquad (20)$$

The two simultaneous equations in expression (20) can be solved for Z_{xx} and Z_{xy}. In a similar manner, another set of equations can be solved for Z_{yx} and Z_{yy}.

Bostick and Smith (1962) proposed an alternative approach in which the Fourier transforms in (20) were replaced by auto-power and cross-power spectra using the Blackman and Tukey (1959) approach. A formulation equivalent to Bostick and Smith's might be written as:

$$\left.\begin{aligned} P^{\mathrm{I}}_{h_x e_x} &= Z_{xx} P^{\mathrm{I}}_{h_x h_x} + Z_{xy} P^{\mathrm{I}}_{h_x h_y} \\ P^{\mathrm{II}}_{h_x e_x} &= Z_{xx} P^{\mathrm{II}}_{h_x h_x} + Z_{xy} P^{\mathrm{II}}_{h_x h_y} \end{aligned}\right| \qquad (21)$$

where from data set I for example, the cross-spectra between the time series $h_x(t)$ and $e_x(t)$ is:

$$P^{\mathrm{I}}_{h_x e_x} = \int_{-\infty}^{\infty} p_{h_x e_x}(\tau)\, \mathrm{e}^{-i\omega\tau}\, \mathrm{d}\tau$$

providing the cross-correlation function is defined as:

$$p^{\mathrm{I}}_{h_x e_x}(\tau) = \lim_{T\to\infty} \frac{1}{T} \int_{-T/2}^{T/2} h_x^{\mathrm{I}}(t) e_x^{\mathrm{I}}(t+\tau)\, \mathrm{d}t$$

The set of equations (21) can be solved for the tensor elements Z_{xx} and Z_{xy}, and a similar set of equations can be solved for Z_{yx} and Z_{yy}.

Grillot (1973) has developed a third variation of this approach by first band-pass filtering each magnetotelluric time series $e_x(t)$, $e_y(t)$, $h_x(t)$, $h_y(t)$ using recursive filters having selectivities on the order of 0.1. Horizontal polarizations of the magnetic field are plotted for different events or bursts of signal. Two events are selected having

different polarizations and a Fourier transform of each component is calculated at the center period of the filter over four cycles of the event. These Fourier coefficients are substituted into eq. 20 to determine the tensor elements.

2.2.2. Estimates from N independent record sets

Sims et al. (1971) describe a procedure for optimizing the estimate of a tensor element if one is provided with a large number of independent record sets. They define the best estimate of Z_{xx} and Z_{xy} in a way that minimizes the mean of the squared differences between the measured electric field component, E_{xj}^{meas}, and the electric field predicted from the magnetic field components through the relation:

$$E_{xj}^{\text{pred}} = Z_{xx}H_{xj} + Z_{xy}H_{yj}$$

where the subscript j denotes the j-th data set. The difference between the measured and predicted electric field is $E_{xj}^{\text{meas}} - E_{xj}^{\text{pred}}$. Multiplying this quantity by its complex conjugate and averaging over N record sets we obtain:

$$\psi = \sum_{j=1}^{N} (E_{xj} - Z_{xx}H_{xj} - Z_{xy}H_{yj}) \cdot (E_{xj}^{*} - Z_{xx}^{*}H_{xj}^{*} - Z_{xy}^{*}H_{yj}^{*}) \quad (22)$$

where each component is the Fourier coefficient of the measured time series. The values Z_{xx} and Z_{xy} that minimize eq. 22 can be determined by first setting the derivative of ψ with respect to the real and imaginary parts of Z_{xx} to zero which leads to:

$$\sum_{j=1}^{N} E_{xj}H_{xj}^{*} = Z_{xx}\sum_{j=1}^{N} H_{xj}H_{xj}^{*} + Z_{xy}\sum_{j=1}^{N} H_{yj}H_{xj}^{*} \quad (23a)$$

Then by setting the derivative of ψ with respect to the real and imaginary parts of Z_{xy} to zero we obtain:

$$\sum_{j=1}^{N} E_{xj}H_{yj}^{*} = Z_{xx}\sum_{j=1}^{N} H_{xj}H_{yj}^{*} + Z_{xy}\sum_{j=1}^{N} H_{yj}H_{yj}^{*} \quad (23b)$$

The two relations (23a, b) can be solved as simultaneous equations to yield the tensor elements Z_{xx} and Z_{xy}. A relation similar to eq. 22 can be formulated to give Z_{yx} and Z_{yy} by minimizing the mean of the squared differences between E_{yj}^{means} and E_{yj}^{pred}.

2.2.3. Estimates using cross-correlation analysis of single record sets

In Fig. 8 we show a model in which two independent stationary random input signals, $x_1(t)$ and $x_2(t)$, are coupled through two linear systems characterized by the impulse response functions $h_1(t)$ and $h_2(t)$, respectively, to produce a third signal $y(t)$ such that:

$$y(t) = \int_{-\infty}^{\infty} h_1(\tau)x_1(t-\tau)\,d\tau + \int_{-\infty}^{\infty} h_2(\tau)x_2(t-\tau)d\tau \quad (24)$$

Tick (1963) describes a method for determining the characteristics of the linear systems, $h_1(t)$ and $h_2(t)$. This, of course, is precisely the time-domain analog of determining the tensor elements which couple two magnetic components to each electric component.

By writing eq. 24 at the lag time $(t+s)$ instead of t, and cross-correlating with $x_1(t)$ we obtain:

$$\lim_{T\to\infty} \frac{1}{T}\int_{-T/2}^{T/2} x_1(t)y(t+s)\,dt =$$

$$= \lim_{T\to\infty} \frac{1}{T}\int_{-T/2}^{T/s} x_1(t)\int_{-\infty}^{\infty} h_1(\tau)x_1(t+s-\tau)d\tau dt$$

$$+ \lim_{T\to\infty} \frac{1}{T}\int_{-T/2}^{T/2} x_1(t)\int_{-\infty}^{\infty} h_2(\tau)x_2(t+s-\tau)d\tau dt \quad (25)$$

Inverting the order of integration we can integrate over t and express eq. 25 in terms of cross-correlation functions of the form of eq. 17a. In this way eq. 25 becomes:

$$p_{x_1y}(s) = \int_{-\infty}^{\infty} h_1(\tau)p_{x_1x_1}(s-\tau)d\tau + \int_{-\infty}^{\infty} h_2(\tau)p_{x_1x_2}(s-\tau)d\tau \quad (26)$$

or, in the frequency domain:

$$P_{x_1y}(\omega) = H_1(\omega)P_{x_1x_1}(\omega) + H_2(\omega)P_{x_1x_2}(\omega) \quad (27)$$

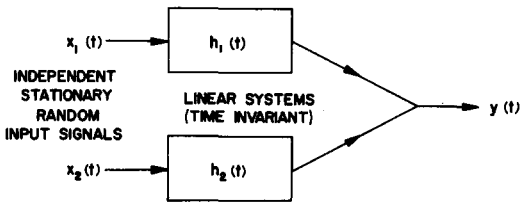

Fig. 8. Time-domain model of two independent signals $x_1(t)$ and $x_2(t)$, combining through two linear systems $h_1(t)$ and $h_2(t)$, to produce a third signal $y(t)$.

where the cross-powers are defined in eq. 17b and $H_1(\omega)$ and $H_2(\omega)$ are the Fourier transforms of the impulse response functions. In a similar way, $x_2(t)$ can be cross-correlated with eq. 24 at the lag-time $(t + s)$ leading to:

$$P_{x_2 y}(\omega) = H_1(\omega) P_{x_2 x_1}(\omega) + H_2(\omega) P_{x_2 x_2}(\omega) \quad (28)$$

Eq. 27 and 28 represent two simultaneous equations which can be solved to yield $H_1(\omega)$ and $H_2(\omega)$, providing the determinant:

$$\begin{vmatrix} P_{x_1 x_1} & P_{x_1 x_2} \\ P_{x_2 x_1} & P_{x_2 x_2} \end{vmatrix} \quad (29)$$

is non-zero. This condition is met if $x_1(t)$ and $x_2(t)$ are independent and randomly correlated.

Madden and Nelson (1964) were the first workers to apply a variation of this technique to estimating the tensor impedance elements. They formulated equations similar to eq. 27 and eq. 28 in terms of the smoothed auto-power and cross-power spectra.

More recently other workers have suggested simulating the smoothed auto-power and cross-power spectral density estimates in eq. 28 by averaging a number of Fourier harmonics over a discrete band of frequencies (Sims and Bostick, 1969; Vozoff, 1972). In this case, tensor elements can be determined from simultaneous equations of the form:

$$\left.\begin{aligned} \langle E_x H_x^* \rangle &= Z_{xx} \langle H_x H_x^* \rangle + Z_{xy} \langle H_y H_x^* \rangle \\ \langle E_x H_y^* \rangle &= Z_{xx} \langle H_x H_y^* \rangle + Z_{xy} \langle H_y H_y^* \rangle \end{aligned}\right| \quad (30)$$

where the brackets denote frequency-band averages of terms like relation (16) as approximations to smoothed power spectral estimates from relations like (17b) for a finite lag. The two terms Z_{xx} and Z_{xy} are, in a sense, average estimates of the tensor elements over the smoothing band-width.

A schematic of an algorithm that we have found useful for frequency-band averaging is shown in Fig. 9. The raw data are first band-pass filtered at the frequency of interest. The filtered data are then replotted both as a set of time series as well as a set of horizontal polarization diagrams for the electric and magnetic components. A visual inspection of these plots can be checked qualitatively for correlation between the magnetotelluric components and for independence between the data sets.

Examples of this technique applied to the two substorms in Fig. 1 are shown in Fig. 10 and 11 where

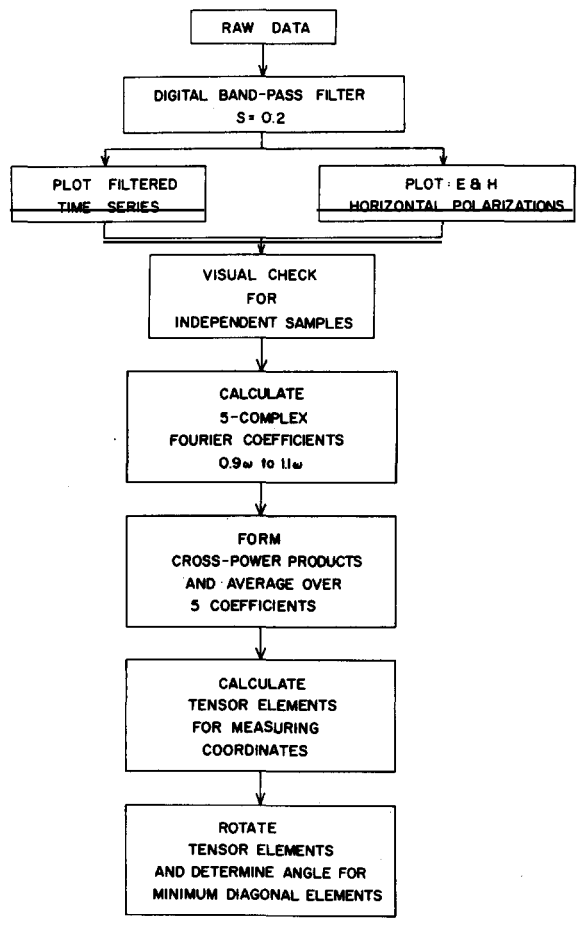

Fig. 9. Schematic of an algorithm for estimating tensor elements using frequency-band averaging.

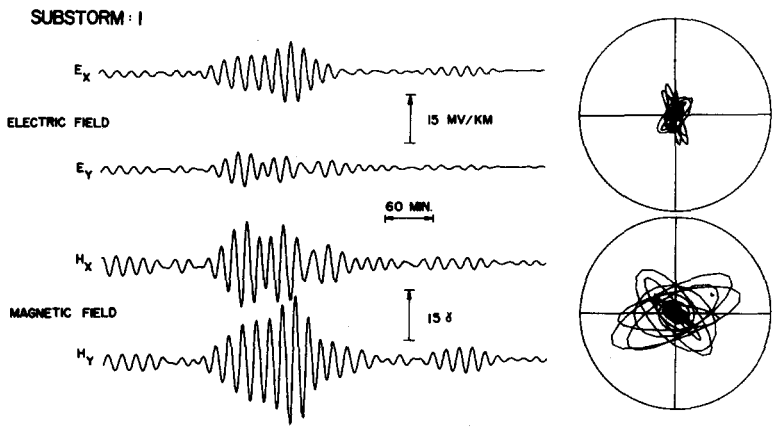

Fig. 10. Band-pass filtered data from substorm 1 (Fig. 1), the polarization plots to the right are for the electric field (top) and for the magnetic field (bottom) to the same scale as the time series.

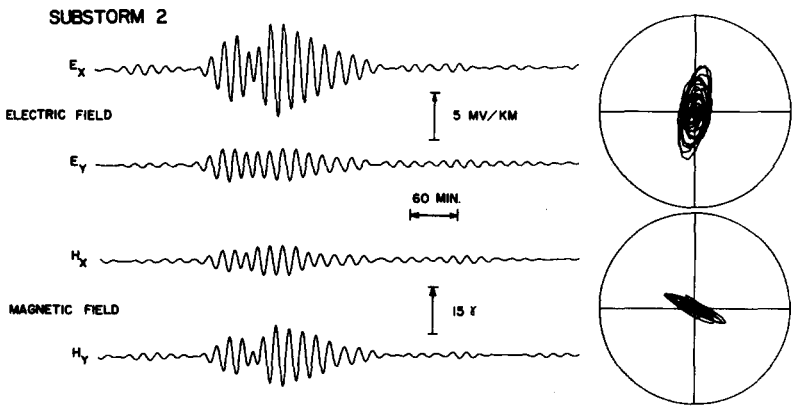

Fig. 11. Band-pass filtered data from substorm 2 (Fig. 1) drawn with the same convention as Fig. 10. Events between orthogonal magnetotelluric pairs (E_x, H_y and E_y, H_x) correlate well. The polarization plots demonstrate a strong linear correlation between E_x, E_y and H_x, H_y.

the raw data have been convolution filtered at 1000-sec period using the frequency response in Fig. 3. Five complex coefficients are determined for each magnetotelluric component at equally spaced frequencies within the band ± 10% of the center frequency. Cross-power products of the coefficients are formed at each frequency and the five complex cross-power coefficients are averaged together as shown in eq. 30. One may solve these two equations for Z_{xx} and Z_{xy}. A similar set of equations can be set up and solved for Z_{yx} and Z_{yy}.

Having calculated the tensor elements for our *measuring* coordinate system, the last step in the algorithm of Fig. 9 is to determine the *principal* coordinate system defined in section 1.3, which is done by rotating the tensor elements and determining the angle that minimizes the diagonal elements. This technique is discussed with two contrasting examples in the next section.

2.3. Determining the principal directions

In section 1.2 it was pointed out that during a coordinate rotation, the tensor elements Z_{xx} and Z_{yy} in eq. 9 go through minima each time the rotating coordinate system (x, y) passes through a principal direction (either x' or y'). Bostick and Smith (1962) applied this feature by actually plotting the

tensor elements as a function of rotation angle, selecting the angles at which the diagonal elements are minimum as the principal directions.

As an example, we show in Fig. 12, the rotation of tensor elements calculated from substorm 1 (Fig. 10) using the algorithm for frequency-band averaging described in section 2.2.3. The rotation of the tensor elements behaves properly as there are two minima in $|Z_{11}|$ and one minimum in $|Z_{12}|$.

On the other hand, tensor elements calculated from substorm 2 do not rotate properly as shown in Fig. 13, since $|Z_{11}|$ goes through only one minimum while rotating through 180°. We might well be suspicious of tensor estimates from substorm 2 since the polarization plot in Fig. 11 suggests a linear correlation between the two electric field components, as well as between the two magnetic field components, which implies that the two magnetic field components are not independent as required for solving equation set (30). The polarization plots of substorm 1 in Fig. 10 show a more random

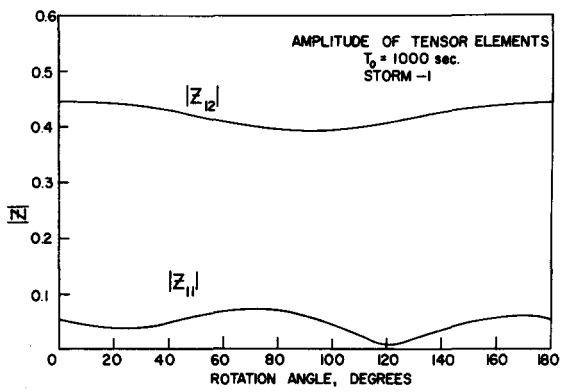

Fig. 12. Amplitudes of tensor elements calculated from substorm 1 as functions of rotation angle. Two minima are apparent in Z_{11} (or Z_{xx}) and one minimum is apparent in Z_{12} (or Z_{xy}).

correlation between the field components; hence this data set provides more reliable estimates of the tensor elements.

Clearly, one must exercise caution not only in using frequency-band averaging techniques to estimate the tensor elements, but in using any of the techniques outlined in section 2.2 since they all require *independent* samples of the magnetotelluric field components. One does well, therefore, to investigate carefully the nature of the data at each stage in its processing.

2.4. Comparison between Cagniard estimates and tensor estimates

In our final example, we contrast apparent resistivity estimates from the Cagniard relation eq. 3 with estimates from the principal values of the tensor impedance eq. 7.

The magnetotelluric components recorded during the substorm in Fig. 6 were band-pass filtered using recursive digital filters with a selectivity of 0.1 at a period of 150 sec. Following the method of Grillot (1973), complex Fourier coefficients were calculated for a number of events selected by inspecting the filtered record section. Each event was four periods or 600 sec long and the entire record was more than 54,000 sec long. Apparent resistivities calculated from the complex Fourier coefficients of each event are given in the left hand columns of Table III where the subscript on the apparent resistivity denotes the sense of the electric field component. The Cagniard

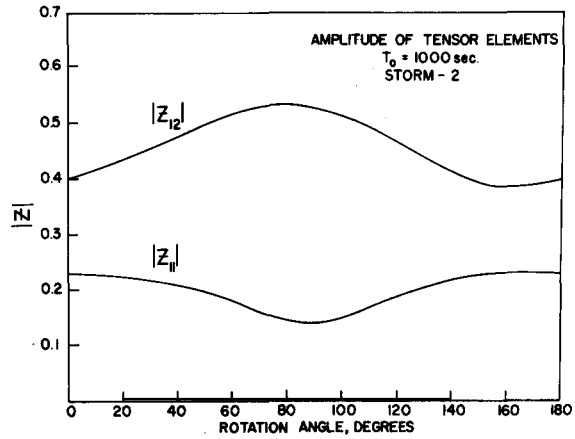

Fig. 13. Amplitudes of tensor elements calculated from substorm 2 as functions of rotation angle. The elements do not properly rotate, as there is only one minimum in Z_{11}, do not two as required.

estimates display a relatively broad range of scatter with a standard deviation of approximately 50% of the mean.

The same complex Fourier coefficients that were used to make the Cagniard estimates were used to determine the tensor elements by solving equations of the form (20) for the event-pairs given in Table III. The tensor elements were rotated to an angle that minimized the diagonal terms, and the apparent resistivities calculated from the principal impedance

TABLE III
Comparison of apparent resistivities calculated from the simple Cagniard relation and from off-diagonal elements of rotated impedance tensor.

Cagniard estimates			Rotated tensor impedance estimates			
Event no.	ρ_x (Ω-m)	ρ_y (Ω-m)	Event pairs	ρ_{xy} (Ω-m)	ρ_{yx} (Ω-m)	Rotation angle (east of North)
5	41	12	5,6	38	18	−5°
6	42	13	6,12	48	21	−15°
7	44	13	7,5	35	18	−10°
8	46	10	8,7	36	21	−10°
11	26	31	11,6	34	19	−5°
12	35	48	12,5	48	19	−15°
13	102	32	13,11	46	16	+15°
14	90	36	14,11	46	18	+15°
15	74	34	15,11	43	17	+10°
	$(\rho_x) = 56$ s.d. = 25	$(\rho_y) = 25$ s.d. = 13		$(\rho_{xy}) = 42$ s.d. = 5.4	$(\rho_{xy}) = 19$ s.d. = 1.8	$(\theta) = -2°$ s.d. = 12°

Site: Sudurarhraun (N. Central Iceland). Period: 150 seconds. Analysis techniques: Complex Fourier coefficients calculated for individual events on filtered record. Coordinates: Geographic.

values (Z'_{xy} or Z_{yx}) are given in the right hand columns of Table III along with the rotation angle.

In comparison with the Cagniard estimates, the rotated tensor impedance estimates clearly separate into two modes with principal resistivities of approximately 20 and 40 Ω-m. The standard deviation is now approximately 10% of the mean, a significant improvement over the range of Cagniard estimates.

A further observation is that by inspecting the column of rotation angles in Table III, it appears that the *principal* coordinate system is more or less aligned along the same direction as the *measuring* axes, which were along geographic coordinates. This implies, for this particular example, that if the earth was indeed strictly two-dimensional then the Cagniard estimates based on field quantities measured in geographic coordinates would separate into maximum and minimum values which were essentially the same as the estimates based on the principal tensor elements. Close inspection of the average Cagniard resistivities in the left-hand columns of Table III does seem to show a tendency which, in retrospect, appears to reflect the tensor estimates in the right-hand columns. However, ρ_x does not precisely equal ρ_{xy}, and moreover ρ_x shows a great deal more scatter than the scatter in ρ_{xy}. This is due to the fact that when calculating ρ_x, one uses the electric field component E_x which, from eq.7, is in a sense contaminated by a contribution from the parallel magnetic field component H_x through the coupling term Z_{xx}. Although this term is small, it nevertheless is not zero, and leads to instabilities in the Cagniard estimates whenever the magnetic field is strongly polarized parallel to the coordinate along which the electric field is measured.

Therefore, it appears that apparent resistivities estimated from the rotated tensor elements should be significantly more stable than estimates from the field ratios themselves (the Cagniard estimate), even when the measured field components are known to lie along the principal coordinates.

3. Conclusion

Determining the nature of the transfer function coupling the telluric and magnetic variation fields is the fundamental problem in the processing of magnetotelluric data. In general this transfer function has a tensor character and one is faced with the problem of

obtaining reliable estimates of tensor elements which are stable from data set to data set, and which vary smoothly with frequency. A number of techniques have been described for transforming time series into the frequency domain. These involve: (1) Fourier harmonic analysis; (2) Fourier transient analysis; (3) power spectral analysis; (4) band-pass filtering.

Moreover a variety of methods are available for manipulating multiple electromagnetic time series to provide estimates of the tensor impedance elements themselves. These are: (1) estimates from two independent record sets; (2) estimates from N independent record sets; (3) estimates using cross-correlation analysis of single record sets.

It has been our impression in using all of these methods that there are strengths and weaknesses in each of them. By the same token, none of the methods is inherently superior to the others. We, ourselves, have tended to discourage "routine" data processing and are more in favor of closely inspecting the data at all stages of the analysis. We place much greater reliance on our results if a number of data processing techniques lead to the same answer. As implied earlier, we feel that considering the empirical nature of magnetotelluric data processing, there is no substitute for having a great deal of physical insight into the nature of the particular data being used.

Acknowledgements

I would like to acknowledge the assistance provided by Larry R. Grillot who was not only an amiable field companion while acquiring the data, but helped enormously in its subsequent analysis.

Support for much of the research above was provided by N.S.F. Grants GA-11850, GA-30101, and GA-26142.

References

Bergland, G.D., 1969. *I.E.E.E. Spectrum,* 6 (7): 41.

Blackman, R.B. and Tukey, J.W., 1959. *The Measurement of Power Spectra.* Dover, New York, N.Y. 190 pp.

Bostick, F.X. and Smith, H.W., 1962. *Proc. Inst. Radio Eng.,* 50: 2339.

Cagniard, L., 1953. *Geophysics,* 18: 33.

Cantwell, T., 1960. *Detection and Analysis of Low-Frequency Magnetotelluric Signals.* Thesis, Geophysics Laboratory, M.I.T., Cambridge, Mass., 171 pp.

Chapman, S. and Bartels, J., 1940. *Geomagnetism.* Oxford University Press, London, 1049 pp.

Cooley, J.W. and Tukey, J.W., 1965. *Math. Comput.,* 19: 297.

Grillot, L.R., 1973. *Regional Electrical Structure beneath Iceland as determined from Magnetotelluric Data.* Thesis, Brown Univ., Providence, R.I., 80 pp.

Hermance, J.F. and Garland, G.D., 1968. *Earth Planet. Sci. Lett.,* 4: 469.

Jenkins, G.M., 1961. *Technometrics,* 3: 133.

Jenkins, G.M. and Watts, D.G., 1968. *Spectral Analysis.* Holden-Day, San Francisco, Calif.

Jury, E.I., 1964. *Theory and Application of the z-Transform Method.* Wiley, New York, N.Y.

Kato, Y. and Kikuchi. T., 1950. *Sci. Rep. Tohoku Univ., Ser. 5, Geophys.,* 2: 139.

Keller, G.V. and Frischknecht, F.C., 1966. *Electrical Methods of Geophysical Prospecting.* Pergamon, New York, N.Y., 519 pp.

Kovtun, A.A., 1961. *Isv. Akad. Nauk S.S.S.R., Ser. Geofiz.,* 1663.

Lee, Y.W., 1963. *Statistical Theory of Communication.* Wiley, New. York, N.Y., 509 pp.

Madden, T., 1964. In: D.F. Bleil (Editor), *Natural Electromagnetic Phenomena below 30 KC/S.* Plenum, New York, N.Y., 429 pp.

Madden, T. and Nelson, P., 1964. *A Defense of Cagniard's Magnetotelluric Method. Project NR-371-401,* Geophysics Laboratory, M.I.T., 41 pp.

Morrison, H.F., Wombwell, E. and Ward, S.H., 1968. *J. Geophys. Res.,* 73: 2769.

Price, A.T., 1950. *Q. J. Mech. Appl. Math.,* 3: 385.

Rikitake, T., 1946. *Bull., Earthquake Res. Inst., Tokyo Univ.,* 24: 1.

Schmucker, U., 1970. *Anomalies of Geomagnetic Variations. Bull. Scripps Inst. Oceanogr.,* 13: 165.

Shanks, J. L., 1967. *Geophysics,* 32: 33.

Sims, W.E. and Bostick Jr., F.X., 1969. *Methods of Magnetotelluric Analysis. Electr. Res. Lab. Tech. Rept. 58,* University of Texas, Austin, Texas, 86 pp.

Sims, W.E., Bostick Jr., F.X. and Smith, H.W., 1971. *Geophysics,* 36: 938.

Srivastava, S.P., Douglass, J.L. and Ward, S.H., 1963. *Geophysics,* 28: 426.

Swift Jr., C.M., 1967. *A Magnetotelluric Investigation of an Electrical Conductivity Anomaly in the Southwestern United States.* Thesis, Geophysics Laboratory, M.I.T., Cambridge, Mass., 211 pp.

Tick, J.L., 1963. In: M. Rosenblatt (Editor), *Time Series Analysis.* Wiley, New York, N.Y., 197 pp.

Tikhonov, A.N., 1950. *Dokl. Akad. Nauk, S.S.S.R.,* 73: 295.

Vozoff, K., Hasegawa, H. and Ellis, R.M., 1963. *Geophysics,* 28: 778.

Vozoff, K., 1972. *Geophysics,* 37: 98.